JOURNAL OF SOLID STATE CHEMISTRY 97, 405–418 (1992)

The Modulated Structure of $Ca_{.85}CuO_2$ as Studied by Means of Electron Diffraction and Microscopy

O. MILAT,*,† G. VAN TENDELOO*,[1] S. AMELINCKX,*
T. G. N. BABU,‡ AND C. GREAVES‡

*University of Antwerp (RUCA), Groenenborgerlaan 171, B 2020 Antwerp, Belgium; †Institute of Physics of the University of Zagreb, Bijenicka 46, 41000 Zagreb, Yugoslavia; and ‡The School of Chemistry, University of Birmingham, Birmingham B152TT, United Kingdom

Received July 15, 1991

The structure of the compound $Ca_{.85}CuO_2$, which was recently determined by neutron and X-ray powder diffractometry, was reexamined making use of electron diffraction and electron microscopy. The general features of the previously proposed model are confirmed. However, the modulated structure, for which only a tentative proposal was made in previous work, was found to be rather different. The calcium distribution along the "tunnels" formed within the CuO_2 framework is responsible for the modulation. The average Ca–Ca separation along these tunnels is found to be different from the Cu–Cu separation along the same direction in the surrounding framework, five calcium spacings corresponding with six copper spacings. This relation explains the complicated stoichiometry. The non-uniform distribution of the calcium along the tunnels causes modulation waves along $(011)_0$ planes, or along the equivalent $(01\bar{1})_0$ planes. The presence of these two symmetry related variants leads to modulation twins.

Introduction

The cuprates have recently become of particular interest in view of the fact that a number of these compounds can be doped so as to become high temperature superconducting materials. In the framework of a study of potential new superconductors, some aspects of the structure of calcium cuprate $Ca_{.85}CuO_2$ were recently determined by X-ray single crystal (*1*) and neutron powder diffraction (*2*). Even though this compound does not seem to look promising as a superconductor, it is of interest since it exhibits a remarkable modulated structure with a complicated stoichiometry. Moreover, it is one of the simple phases occurring in the phase diagram of the complex superconductors based on bismuth and thallium.

In view of the uncertainty relating to the details of the superstructure of this material, it was judged desirable to confirm it by means of high resolution electron microscopy and electron diffraction, which are particularly suited to study modulated structures provided the basic structure is known. In this sense, electron microscopy is a complementary technique to the other diffraction techniques.

In this paper we show that although the

[1] To whom correspondence should be addressed.

0022-4596/92 $3.00

general features of the structural models previously described (*1*, *2*) are confirmed, the modulated structure, as deduced from the high resolution images and electron diffraction patterns, differs in some details from those previously proposed.

Structure Considerations

A number of calcium cuprates having different compositions and crystal structures (*1–6*) were recently synthesized (*1*, *2*, *5*, *6*) in view of their potential role in the development of new high T_c superconductors. Among these compounds $CaCuO_2$ is of particular interest since it occurs in slabs having this composition in the $Bi_2Sr_2Ca_nCu_{n+1}O_{2n+6}$ and $Tl_2Ba_2Ca_nCu_{n+1}O_{2n+6}$ families of high T_c superconductors.

The compound $Sr_{0.14}Ca_{0.86}CuO_2$ was found to have a tetragonal structure (*6*) but the pure calcium cuprate turns out to have the same Ca/Cu ratio, i.e., to be nonstoichiometric, with composition $Ca_{0.85}CuO_2$ and to have an orthorhombic structure with lattice parameters: a_0 = 0.6324 nm; b_0 = 0.2807 nm; c_0 1.0573 nm.

The proposed structure consists of a lattice of edge sharing CuO_4 square planar groups situated in planes parallel with $(100)_0$ and forming CuO_2 ribbons parallel with the b_0 axis, Fig. 1. The copper atoms, which are the centers of these planar groups, form a face-centered orthorhombic Bravais lattice. As a result of the edge sharing, the oxygen atoms form strings, parallel with b_0, of somewhat deformed interpenetrating octahedra. These octahedra are partially occupied by Ca atoms. If one out of two of the centers of these octathedra would be occupied the composition of the crystal would be $CaCuO_2$, and the filled octahedra would be sharing edges. It was suggested (*2*) that only 0.425 of such sites are occupied leaving roughly seven in twelve sites vacant. The vacancies were assumed to be concentrated in planar interfaces parallel with $(110)_0$. The

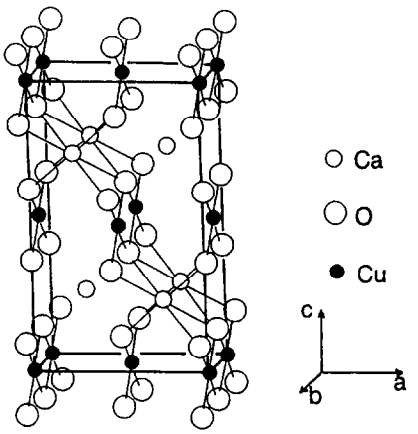

FIG. 1. The orthorhombic subcell of $Ca_{.85}CuO_2$, after (*1*).

presence of the vacancies causes displacements of the Ca atoms out of the centers of the oxygen octahedra so as to realize a more uniform distribution and to allow relaxation of the adjacent oxygen atoms. An alternative, related model suggested that the partial occupancy of the Ca sites results in a variety of superstructures along [010], e.g., $b = 5b_0$, $10b_0$, $12b_0$ (*1*).

Experimental

$Ca_{.85}CuO_2$ material was synthesized in the form of a fine powder by Babu and Greaves (*2*). Samples suitable for electron microscopy investigation were prepared simply by further crushing so that "beam transparent" thin areas were found along the grain edges. The tilting goniometer stage of a conventional 100C electron microscope was used for reciprocal lattice inspection, and a high-resolution 4000EX microscope for HREM imaging.

Electron Diffraction Patterns

The most relevant diffraction patterns are shown in Fig. 2. Those spots which can be consistently assigned orthorhombic indexes

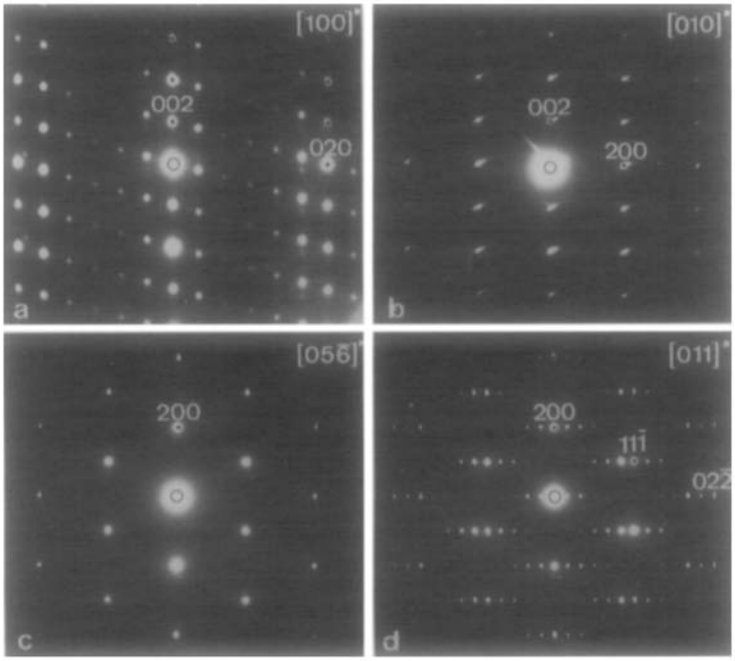

FIG. 2. Electron diffraction patterns of $Ca_{.85}CuO_2$ along different zones. The indices refer to the basic orthorhombic lattice; (a) $[100]_o^*$ zone; (b) $[010]_o^*$ zone; (c) $[056]_o^*$ zone; (d) $[011]_o^*$ zone.

are considered as main or basic spots. The patterns of Fig. 2(a) and Fig. 2(d) exhibit basic spots, as well as satellite sequences associated with them. In Fig. 2(b) only basic spots are present which can be indexed unambiguously as a $[010]_o$ zone pattern. The projected structure along this zone is centered since only reflections with h = even and l = even are present; since there are no satellites in this section of reciprocal space, it can be concluded that the projection along this zone only reveals the basic structure. Atom displacements due to modulation must thus either have components along the $[010]_o$ direction only, or in any case be such as not to give rise to a superperiod in the (a_o, c_o) plane.

Figure 2(d) shows the $[011]_o$ zone pattern; it consists of linear arrays of satellites parallel with $[01\bar{1}]_o$, each containing 12 spots of which the intensity decreases with distance away from the center of the array. The "centers of gravity" of these arrays, localized close to the most intense spots, form a centered rectangular arrangement which can be indexed as basic reflections, indicated in Fig. 2(d). The satellite spacing corresponds with an interplanar spacing of about 12 d_{022}.

The arrays of satellites are not always exactly parallel with $[01\bar{1}]_o$; moreover their spacing is sometimes not exactly $\frac{1}{12}[02\bar{2}]_o$, i.e., the diffraction patterns may exhibit spacing and (or) orientation anomalies, Fig. 3. When considering satellites associated with successive basic reflections, as they are indicated in Fig. 3(a) above and below the row, they do not coincide exactly. In Fig. 3(a) only a spacing anomaly is visible, while in Fig. 3(b) also an orientation anomaly is obvious, i.e., rows of satellites enclose a small angle with the direction between basic reflections. It is found that these anomalies may depend on the part of the foil selected for the diffraction experiment. These

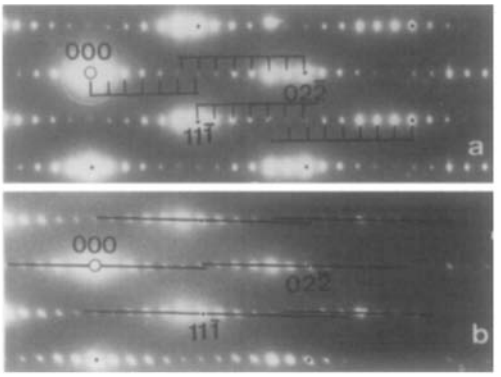

FIG. 3. Part of diffraction patterns along the $[011]_o^*$ displaying: (a) a small spacing anomaly; (b) a small orientational anomaly.

observations suggest that the structure is incommensurate with a variable incommensurability.

Figure 2(a) shows the $[100]_o$ zone as indexed with respect to the orthorhombic lattice. This $[100]_o$ zone is remarkable in two respects: (i) the satellite spacing along $[01\bar{1}]_o$ is doubled as compared to that in Fig. 2(d), and moreover, (ii) there are satellite arrays along two twin related directions. The presence of twin spots is more pronounced in the pattern of Fig. 4, made along the same $[100]_o$ zone but from an area of the crystal where both twins were present in unequal fraction. The presence of two directions of the satellite sequences, Fig. 4, reveals the presence of modulation twins with a $(001)_o$ mirror plane.

The doubling of the satellite spacing is a consequence of systematic extinctions, as can be concluded from a tilting experiment about an axis $[01\bar{1}]_o$, parallel with the satellite rows, Fig. 5. The weak spot appears in between the satellites in Fig. 5(a) as soon as, due to tilting out of the $[100]_o$ zone, the rows from an inclined section intersect Ewald's sphere, Fig. 5(b). In Fig. 5(b), the odd numbered satellites in the $[011]_o$ row are systematically weaker than the even numbered ones, which confirms that they are presumably due to multiple diffraction violating the extinctions. In the $[100]_o$ zone the odd numbered satellites become extinct.

The $[05\bar{6}]_o^*$ zone pattern of Fig. 2(c) intersects the linear arrays of satellites along a plane of the $[100]_o$ zone, passing through the strong satellite spot indicated as $10\ 0\ 4_m$ in Fig. 6(a) and thus, it is an oblique section that exhibits no satellite sequences.

The incommensurability of the diffraction patterns being small and variable it is justified, as a first approximation, to use a description of the complete diffraction patterns based on a commensurate monoclinic superlattice with parameters

$$\begin{bmatrix} \mathbf{a}_m \\ \mathbf{b}_m \\ \mathbf{c}_m \end{bmatrix} = \begin{bmatrix} 0 & 6 & 0 \\ 1 & 0 & 0 \\ 0 & -1 & 1 \end{bmatrix} \begin{bmatrix} \mathbf{a}_o \\ \mathbf{b}_o \\ \mathbf{c}_o \end{bmatrix}$$

The lattice of the twin is then given by the base vectors $\mathbf{a}'_m = \mathbf{a}_m$; $\mathbf{c}'_m = -\mathbf{c}_o - \mathbf{b}_o$; $\mathbf{b}'_m = \mathbf{a}_o$.

With respect of this superlattice the $[100]_o = [010]_m$ diffraction patterns in Fig. 2(a) and $[011]_o = [001]_m$ in Fig. 2(d), can be indexed

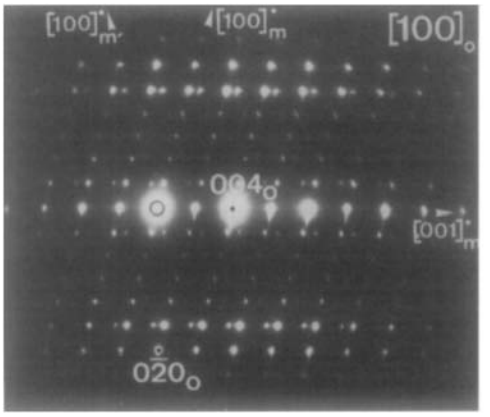

FIG. 4. $[100]_o^*$ zone diffraction pattern of a twinned crystal of $Ca_{.85}CuO_2$. The subscript "o" refers to the basic orthorhombic lattice, whereas the subscript "m" refers to the monoclinic modulated superstructure. The $(001)_o$ plane is a mirror plane.

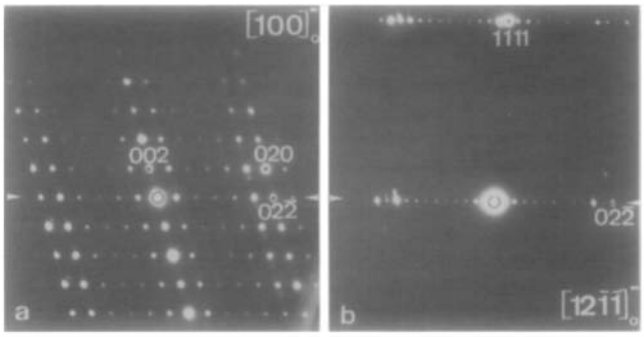

FIG. 5. Comparison of the $[100]_0$ and the $[12\ \bar{1}\ \bar{1}]_0$ zone pattern obtained by tilting around the $[02\bar{2}]_0^*$ rotation axis. Note that in (a) the satellite spacing is twice that in (b) due to systematic extinction. The odd numbered satellites in the $[022]_0^* = [100]_m^*$ row of (b) are systematically weaker than the even numbered ones, showing that the odd numbered ones must be due to double diffraction.

as indicated in Fig. 6(a); we note the diffraction conditions: $h0l$ are present for h = even and $h00$ for h = even. In sections, other than $(010)_m^*$ the spots $h00$ with h = odd are present, e.g., Fig. 5(b), Fig. 2(d), but this must be attributed to double diffraction. The reciprocal lattice as determined from the different sections is represented schematically by top and side projections in Fig. 6(a), and the resulting monoclinic direct lattice unit cell in Fig. 6(b).

High Resolution Images

The high resolution images have been of considerable help in elucidating the modulated structure, assuming the basic structure to be that previously proposed (*1*, *2*).

Figure 7 shows the high resolution image made along the $[011]_0$ zone. It clearly reveals the centered rectangular lattice of the basic structure as an array of bright dots of which the brightness varies periodically along the $[0\bar{1}1]_0$ direction. There are, on the average, somewhat more than five bright dots in one period; in some areas a single-period may contain six bright dots, as indicated by small white arrows in Fig. 7.

The thinnest parts in the wedge shaped specimen of Fig. 7 only reveal one, unmodulated pseudo-hexagonal lattice, as can be judged from the absence of satellites in the optical diffraction pattern of the HREM negative, reproduced as inset (A). At slightly larger thickness the modulation become quite apparent in the image and the optical diffraction pattern in the inset (B) clearly demonstrates this by the presence of satellite sequences with the same geometry as the electron diffraction pattern of Fig. 2(d). The geometry of the bright dot pattern suggest that in the very thinnest part the bright dots reveal copper columns, whereas at larger thickness the bright dots represent calcium columns. This can be deduced from the fact that the same distance, indicated by the pair of parallel black lines in Fig. 7, comprises seven bright dots (i.e., six spacings) in the thin part against six bright dots (i.e., five spacings) in the thicker part; the transition being very gradual. This thickness dependence of the contrast can be understood on the basis of the atomic column approximation (*7*). According to this model, the focusing depth of copper columns (copper having a larger atomic number Z = 29) is smaller than that of calcium columns (Z_{Ca} = 20), and thus the images of copper columns become bright dots at a smaller thickness than the calcium ones. The optical

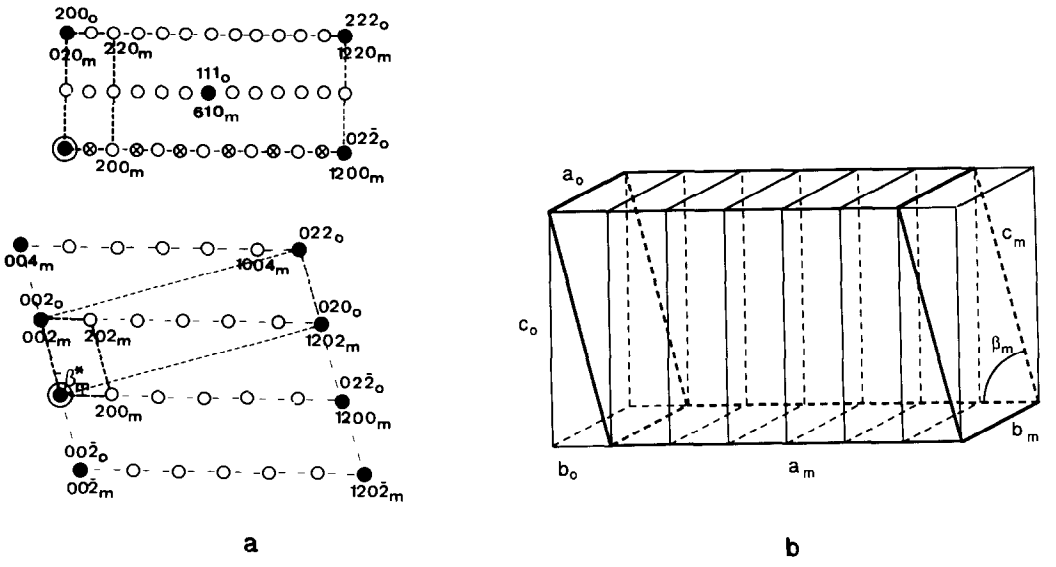

FIG. 6. Schematic representation of monoclinic superlattice cell in reciprocal, (a), and direct, (b), space. Two relevant sections of reciprocal space are indexed by orthorhombic, subscript "o"; and monoclinic, subscript "m" indices. Spots indicated by "x" are extinct for the $[100]_o$ zone due to symmetry, but are excited for the other zones due to double diffraction.

diffraction patterns thus allow one to conclude that the copper sublattice is practically unmodulated, whereas the calcium sublattice is clearly modulated. At some intermediate thickness both copper and calcium columns are imaged simultaneously: the calcium columns as the brightest dots, the copper columns as weaker bright dots. This is indicated schematically in Fig. 7(C), which also demonstrates the lateral shift of the close packed rows of bright dots along the "interfaces" (i.e., the darker fringes in Fig. 7(C). Whereas the lattice of weaker dots (i.e., the copper columns sublattice) is practically unperturbed, by the interfaces the close-packed rows of the sublattice of bright dots suffer a lateral shift at each interface. This lateral shift is due to the fact that the rows of brightest dots (i.e., the calcium columns) perpendicular to the modulation fringes, are not equidistant but have a somewhat larger spacing in the dark fringes. This again confirms that the modulation of the copper sublattice is much smaller than that of the calcium sublattice.

An equally relevant high resolution image is that made along the $[100]_o$ zone, shown in Fig. 8. Along this zone the columns of copper and of calcium atoms can just be resolved and their respective positions deduced, Fig. 8(a). The projected separation of the copper columns being only 0.14 nm, it was necessary to optimize the resolution of the microscope by tilting the incident beam so as to make the projection of the centre of Ewald's sphere coincide with the reciprocal lattice position $01\bar{1}$; in this case the angle-dependent aberrations of the microscope are minimized. The closely spaced rows of bright dots, parallel with the $[010]_o$ direction, and which are clearly resolved close to the edge of the foil, represent alternatingly copper and calcium columns, as indicated on the image, Fig. 8(a). Oxygen columns are not revealed under the conditions used in Fig. 8.

In the thicker part of the specimen the brightness variations reveal the modulation waves. The orientation and periodicity of these brightness variations are consistent with the geometry of the sequences of satellite spots in the diffraction pattern of corresponding zone, Fig. 2(a), assuming all intensity maxima (or minima) to represent equivalent "interfaces."

Counting the number of bright dots in adjacent rows, as indicated in the image reproduced in Fig. 8(a), it is found that on the average six copper columns correspond with only five calcium columns in the adjacent row. This clearly proves that the nonstoichiometry is indeed related to the fact that less than half of the oxygen octahedra are occupied by calcium. It should be noted that as far as can be judged from the high resolution image of Fig. 8(a), the separation of the calcium columns is rather uniform under the contrast condition used. However, brightness modulations in the thicker part of the specimen suggest that there are periodic variations in the detailed local structure. Also, for a certain thickness as in the right part of Fig. 8(a), the rows of bright dots become visibly wavy with a wavelength equal to six times the distance between copper columns.

In Fig. 7 the intensity variation images a period corresponding with the "real" period, i.e., with that of the structural modulation; it corresponds with the inverse of the satellite spacing as observed in the diffraction pattern of Fig. 2(d).

Under different imaging conditions, such as in Fig. 9, it becomes clear that this period comprises in fact two "interfaces," i.e., two different domain strips occur in one period; they are imaged slightly differently. The strips revealed in the image of Fig. 8(a), and the fringes in Fig. 8(b), correspond with the spacing between successive "interfaces," which is only half the real modulation period, in agreement with the extinctions of the odd numbered satellites in the diffraction pattern along this zone. The broad brightness modulations, indicated by white arrows in Fig. 8(a), become the most prominent feature in the dark field image at much smaller magnification in Fig. 8(b). This fringes clearly reveal the presence of modulation twins, in accordance with the diffraction pattern of Fig. 4.

The orthorhombic basic unit cell, as well as the monoclinic superstructure unit cell are both outlined on the image of Fig. 8(a), indicating copper and calcium columns by different dots.

Model

Our observations confirm the general structural features previously proposed (*1*, *2*), i.e., that the structure consists of a lattice of CuO_2 ribbons "stuffed" with calcium atoms. The arrangement of the CuO_2 ribbons gives rise to "tunnels" along b_0, formed by oxygen atoms; we assume this sublattice to be undeformed to a first approximation. The oxygen atoms form strips of somewhat irregular oxygen octahedra which interpenetrate as shown schematically in Fig. 10. In such a string, octahedra with two different orientations alternate. One octahedron such as ACEDBF will be said to be pointing "up" when viewed along the $[100]_0$ zone, whereas the adjacent octahedron CGEDFH will be denoted as pointing "down." Halfway between the centers of successive interpenetrating octahedra is a position such as T which can be considered as the center of a deformed tetrahedron CDFE. Along the "tunnels" there are thus several sites which are symmetry positions and where the size of the interstices presents a relative maximum and therefore are potential locations for inserted calcium atoms.

One can envisage different distributions of calcium atoms along the "tunnels." The one extreme assumption would be that they occupy periodically five successive octahedral sites of the same orientation, leaving

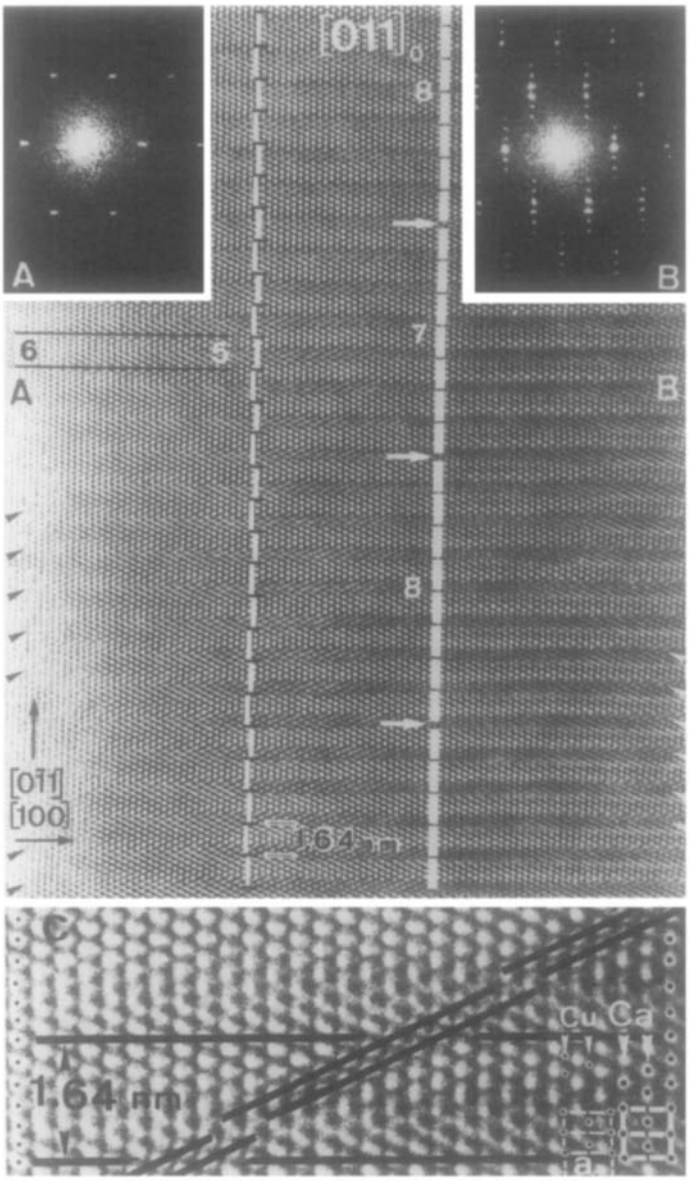

FIG. 7. High resolution image of $Ca_{.85}CuO_2$ along the $[011]_o$ zone axis. Optical diffraction patterns of regions A and B of the negative are shown as insets. Note that in region A the copper sublattice, whereas in region B the calcium sublattice is prominently imaged. The high magnification inset C shows the lateral shift of the rows of dots representing calcium columns. The arrows at edges draw the attention to these shifts at lower magnification. Note the "phase-slips," indicated by white arrows, occurring after 7 or 8 periods of the modulated structure.

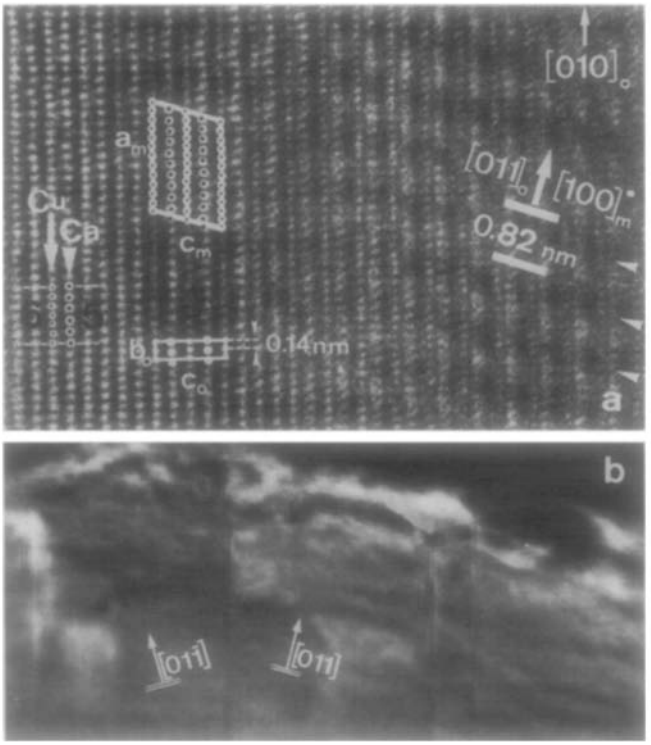

FIG. 8. (a) High magnification high resolution image of $Ca_{.85}CuO_2$ along the $[100]_o$ zone revealing well separated copper (indicated by smaller dot) and calcium (indicated by larger dot) rows of columns. Note that six copper–copper separations correspond with five calcium–calcium separations. Bands of contrast are parallel with $(100)_m$ superlattice planes. (b) Low magnification high resolution dark field image revealing superlattice modulation fringes in twined domains.

every sixth interstice empty, Fig. 11(b). The alternative extreme would be a uniform equidistant distribution of five calcium atoms over a length of "tunnel" equal to six copper–copper spacings, Fig. 11(a). The truth is probably somewhere in between. Due to their mutual repulsion, the calcium ions tend to be uniformly distributed, but on the other hand high symmetry sites are favored on bond energy grounds. The actual configuration is a compromise between these two tendencies, and it is to be expected that the distribution will be slightly non-uniform but quasi-periodic, with an average period which need not be simply related to the Cu–Cu separation in the framework. One furthermore expects that the two types of octahedra will be occupied with equal probability. The Ca configurations in successive $\mathbf{b}_o$ rows along $\mathbf{c}_o$ are clearly correlated, since sharp superlattice spots are produced. In our model, we assume that they are related by a shift over $\frac{1}{2}(\mathbf{b}_o + \mathbf{c}_o)$ (or $\frac{1}{2}(-\mathbf{b}_o + \mathbf{c}_o)$). This is a consequence of the fact that successive rows of oxygen octahedra, which ultimately determine the Ca positions, are shifted over this vector as a result of the face centered arrangement along the $[100]_o$ zone. Whereas these shifts are both symmetry operations for the CuO_2 framework, this is not the case for the Ca configurations, since their repeat distance along the row is $6\mathbf{b}_o$. Also, whereas the two shifts $\frac{1}{2}(\mathbf{b}_o + \mathbf{c}_o)$ or $\frac{1}{2}(-\mathbf{b}_o + \mathbf{c}_o)$ are equiva-

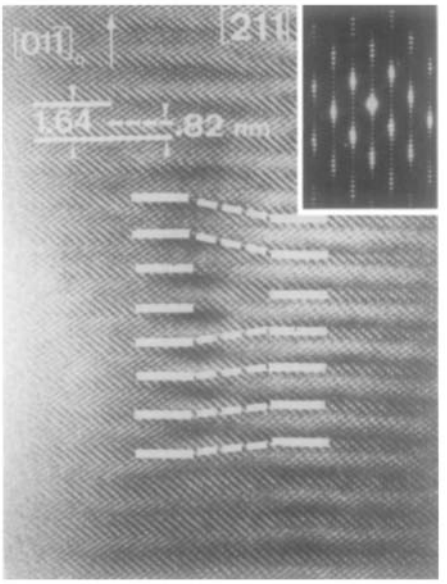

FIG. 9. High resolution image of $Ca_{.85}CuO_2$ along the $[211]_o$ zone revealing that in one period of the modulated structure two strips with a differently oriented strip pattern occur giving rise to a "chevron" pattern. Note also the presence of a "dislocation" like defect in the modulation pattern.

lent for the CuO_2 framework, they lead to twin related crystals if the Ca configurations are taken into account.

In successive rows along the a_o direction the calcium atoms will tend to occupy all interstices of the same orientation, since this ensures the most uniform distribution, but again the actual configuration will be a compromise.

The $[100]_o$ diffraction pattern, Fig. 2(a) as well as the image along this zone, Fig. 8, suggest that the planes of "equal phase" of the modulation, as determined by the Ca configurations, are $(011)_o$ and $(0\bar{1}1)_o$ planes. These considerations suggest the model represented by the two extreme configurations in Fig. 11.

This model also accounts for the twin formation since $(011)_o$ and $(0\bar{1}1)_o$ are equally probable "interfaces" or planes of equal phase. According to this model successive "interfaces," as indicated by heavy dashed lines in Fig. 11(a) and (b), are not equivalent as can be seen in the top projections, lower parts of Fig. 11, representing one c layer of the structure. However, when viewed edge on along the $[100]_o$ zone, upper parts of Fig. 11, their projections are the same, i.e., they become equivalent explaining why the rows of satellite spots have a double spacing in this zone, (Fig. 2(a)). Alternatively, from $[001]_o$ projections we can deduce the presence in the model of a glide mirror plane parallel with $(100)_o$ or $(010)_m$ and with a glide vector $3\mathbf{b}_o$ (i.e., $\frac{1}{2}\mathbf{a}_m$), and thus conclude that the superstructure spots of the type $h0l_m$ should exhibit extinctions for h odd, as observed in Fig. 5(a). Conversely, one could have concluded from the diffraction conditions of the superstructure spots that a mirror glide plane $(010)_m$ with glide vector $\frac{1}{2}\mathbf{a}_m$ should be present in the superstructure.

Image Simulations

Since different arrangements of the calcium atoms have been envisaged it is of interest to compute images for these different models and compare them with the observed ones. Images were obtained for different defocus values, -20, -50, -80 nm, and for different thicknesses ranging from 1.05 to 10.5 nm; they were computed using the direct space method developed by Van Dyck and Coene (*8*).

Three different models with Ca/Cu ratio 5/6, i.e., for composition $Ca_5Cu_6O_{12}$ (or $Ca_{.833}CuO_2$), were considered. In Model I the calcium atoms are equally spaced along the tunnels; in Model II the calcium atoms occupy five successive octahedral interstices, the sixth interstice being left vacant. In Model III the arrangement is a compromise between these two extremes. The three calcium configurations are schematically compared in Fig. 12. In the three cases the patterns of the calcium chains in successive

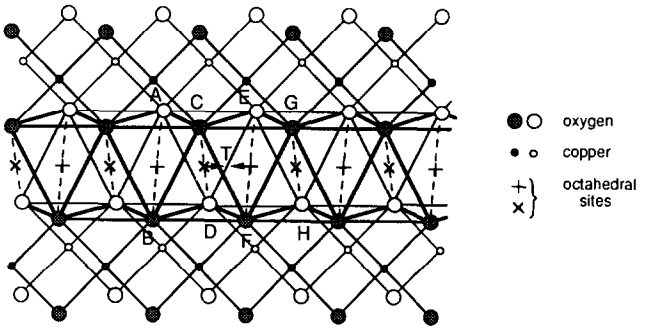

FIG. 10. Framework of four strips of edge sharing CuO_4 squares forming a "tunnel" of interpenetrating octahedra along the b_0 direction of the basic lattice of $Ca_{.85}CuO_2$. Ca atoms occupy the interstitial sites within the "tunnel." Each site in the center of an octahedron, e.g., ACEBDF, is simultaneously in the middle of an edge of the CEGDFH octahedron. The tetrahedral sites T are half way in between two adjacent octahedral sites.

tunnels along the $[001]_0$ direction are related by a vector $\mathbf{b}_0 + \mathbf{c}_0$.

Figure 13 compares the computed images for the three models at -50 and -80 nm defocus and for six different thicknesses. For the smallest thickness, 1.05 nm, the bright dots form a pseudo-hexagonal pattern, which for Model II exhibits extra bright dots due to the vacancies. At somewhat larger thickness, 10.5 nm, a "chevron" pattern becomes visible in the computed images. Comparing the three sets of computed images for increasing thickness with the observed dot pattern in the wedge shaped crystal of Fig. 7, it becomes evident that Model II can be excluded. The choice between Models I and III is less obvious.

Shifts which closely resemble the observed ones in Fig. 8 are found in the computed images for thicknesses ranging from 2.1 to 10.6 nm, defocus -50 to -80 nm, for Models I and III, when viewing Fig. 13 at grazing angle. For larger thicknesses the correspondence between computed and observed image becomes less striking. This is related to the fact that the computational method becomes less reliable at larger thickness. Nevertheless, with increasing thickness the computed images exhibit a tendency to produce two distinct bands in one period in accordance with the observations in the right part of Fig. 7. From this comparison it seems justified to conclude that the calcium atoms must be close to uniformly spaced along the "tunnels"; the localized vacancy—Model II can be excluded.

Discussion

The observations were shown to be consistent with a model in which the modulation is attributed to the arrangement of the calcium atoms in a nearly rigid framework of CuO_2 ribbons. The observed superspacing is the smallest common multiple of the two coexisting basic periodicities; that of the CuO_2 framework and that of the Ca arrangement. In particular, the superspacing is equal to six times the Cu–Cu spacing of the CuO_2 sublattice, which is the same as five times the average Ca–Ca separation, in the commensurate approximation. The structure can be compared with the modulated structure of the non-stoichiometric manganese silicides $MnSi_{2-x}$, in which a rigid framework of manganese is "stuffed" with silicon atoms in a double helix arrangement (*9*).

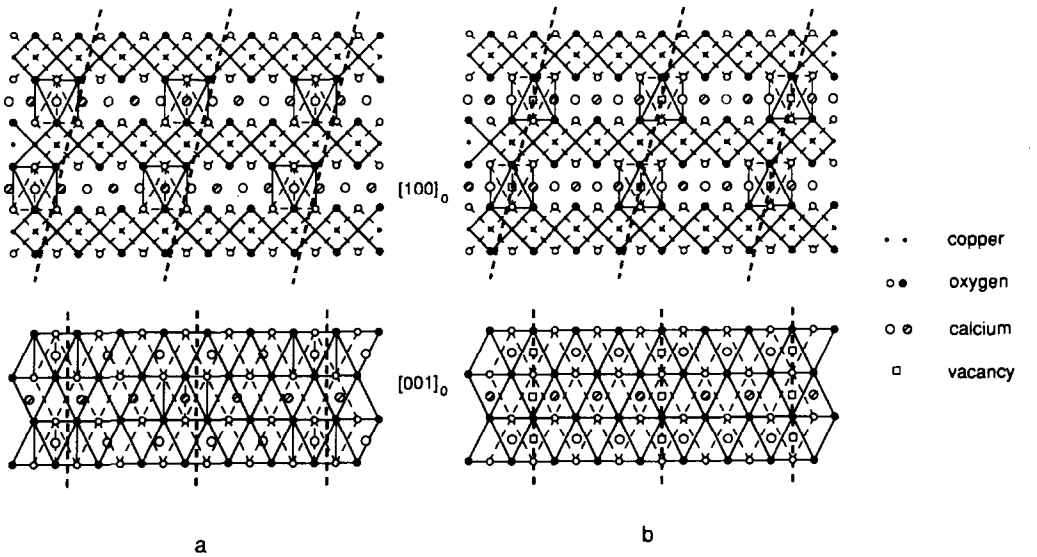

FIG. 11. Models of the modulated structure in $Ca_{.85}CuO_2$ as viewed along the $[100]_0$ zone, above, and along the $[001]_0$ zone, below. (a) Arrangement of Ca atoms with uniform spacing matching five Ca–Ca distances with six Cu–Cu distances; (b) arrangement of Ca atoms in octahedral sites leaving periodically a vacancy.

At high temperature the arrangement of the calcium atoms in the "tunnels" is likely to become uniform, whereas at sufficiently low temperature the tendency to occupy the centers of octahedral interstices presumably dominates. The two extreme models discussed above thus presumably occur both in the appropriate temperature ranges. On lowering the temperature it is then possible that the Ca arrangement is "frozen-in" with different "phases" in different parts of the specimen leading to the formation of "phase-slips" or discommensurations. In Fig. 7 such "discommensurations" can be detected by carefully counting the numbers of bright dots over a number of periods marked by darker lines. Most strips contain five rows of bright dots but periodically a strip containing six dots occurs. These phase slips are not well localized but counting a sufficient number of periods it is found that on the average, one "phase slip" occurs in every seven or eight periods. The density of discommensurations is directly related to the incommensurability deduced from the corresponding diffraction pattern (i.e., to the spacing anomaly). Since the discommensurations accommodate Ca atoms, they also affect the composition. From the average separation of these discommensurations (one in eight or seven strips) as observed along the $[011]_0$ zone, Fig. 7, one finds that

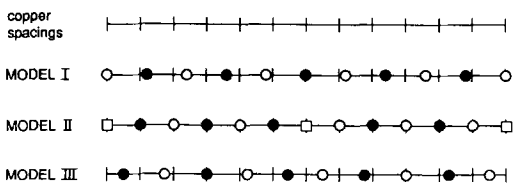

FIG. 12. Schematic comparison of three different Ca atom arrangements used in the image simulation experiments. The bars indicate the copper positions, whereas the open and closed circles indicate the Ca atom positions as projected along the $[100]_0$ direction (c.f., Fig. 11): Model I, equidistant spacing; Model II, five filled octahedra followed by vacancy; Model III, modulated arrangement due to relaxation, i.e., a compromise between I and II.

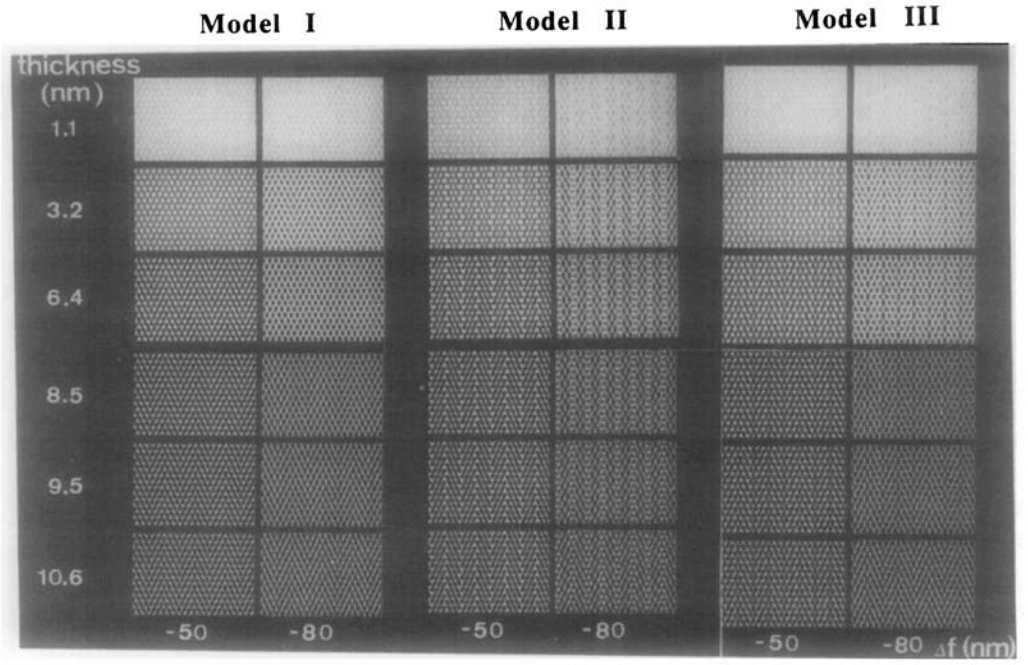

FIG. 13. Simulated images along the $[100]_o$ zone of the three models (see text) for the structure of $Ca_{.833}CuO_2$. Defocus and thickness are indicated in nm for the various images.

the Ca/Cu ratio becomes either 41/48 [(7 × 5 + 1 × 6)/((7 + 1) × 6) = 0.857], or 36/42 [(6 × 5 + 1 × 6)/((6 + 1) × 6) = 0.854], which is closer to the chemically determined Ca/Cu ratio of 0.85 than is 5/6 in the absence of discommensurations.

It is possible to consider an average structure and associated with it an average lattice for the calcium arrangement. This lattice would be face-centered like the basic, orthorhombic one, but slightly deformed so that the parameters, expressed in terms of the orthorhombic ones, would be: $\mathbf{a}_{Ca} = \mathbf{a}_o$; $\mathbf{b}_{Ca} = 6/5\ \mathbf{b}_o$; $\mathbf{c}_{Ca} = \mathbf{c}_o + 1/5\ \mathbf{b}_o$; $\alpha_{Ca} = 87°$. The actual calcium arrangement would then be a displacement modulated variant of this average structure. It is interesting to note that the four strong powder diffraction lines, which could not be indexed on the basis of the orthorhombic cell (*2*), acquire very simple indices when indexed with respect to the average Ca cell. These four lines with interplanar spacing 0.289, 0.282, 0.232, and 0.222 nm, and respective monoclinic superlattice indices 510_m, 512_m, $\bar{5}12_m$, and 514_m, acquire the Ca average sublattice indices 111_{Ca}, $\bar{1}11_{Ca}$, 311_{Ca}, and $\bar{3}11_{Ca}$, respectively.

The exceptionally strongly anisotropic thermal parameter B_{22} of calcium in the orthorhombic structure (*1, 2*) can now be related to the uncertainty in the positions along the "tunnels." The presence of static disorder in the Ca strings can also be concluded from the image of Fig. 7, where the lines of equal phase are not strictly periodic; their positions are essentially determined by the Ca arrangement.

Conclusions

The structure of $Ca_{.85}CuO_2$ can be described as a three dimensional framework, formed by ribbons of edge sharing planar CuO_4 groups "stuffed" with calcium atoms

along the "tunnels" formed within this framework by the oxygen atoms. Due to the large size of the calcium atoms, as compared to the interstices available in such a framework, not all geometrically equivalent sites can be occupied along these "tunnels" and non-stoichiometry and incommensurability results. The image simulations suggest that the calcium atoms are not quite uniformly distributed in the "tunnels."

The structure proposed here differs from that presented in a previous paper (*2*), in particular with respect to the calcium arrangement. The "planes of equal phase" of the calcium and vacancy arrangement were assumed to be $(110)_0$ planes (*2*); they were materialized in a sense by the presence of localized vacancies in these planes. Our observations demonstrate that the "modulation waves" are in fact parallel with $(011)_0$ or $(01\bar{1})_0$ planes. This could be concluded unambiguously from the directions of the rows of the superstructure spots in the diffraction patterns. Our model is consistent with all the electron microscopic results; moreover, it explains in a simple manner the non-stoichiometry and the large value of the anisotropic thermal parameter B_{22}, and allows one to index the strong diffraction peaks left unidentified in Ref. (*2*).

It would be of interest to observe the changes in the calcium arrangement with temperature. It is likely that at high temperature a uniformly spaced arrangement will form, i.e., the "vacancy" will be smeared out. On the other hand, at low temperature the calcium atoms may become more localized. These phenomena are now being investigated.

Acknowledgments

One of us (O.M.) thanks C. Fanidis for a substantial help in performing the image simulation experiments. This work was supported by the Incentive Program on High T_c Superconductors initiated by Belgian State Science Policy Office under contract SU/03/017.

References

1. T. Siegrist, R. S. Roth, C. J. Rawn, and J. J. Ritter, *Chem. Mater.* **2,** 192 (1990).
2. T. G. N. Babu and C. Greaves, *Mater. Res. Bull.* **26,** 499 (1991).
3. C. L. Teske and Hk. Müller-Buschbaum, *Z. Anorg. Allg. Chem.* **370,** 134 (1969).
4. C. L. Teske and Hk. Müller-Buschbaum, *Z. Anorg. Allg. Chem.* **379,** 234 (1970).
5. I. Gazawa, N. Terada, K. Matsutani, R. Sugise, M. Jo, and H. Ihara, *Japan J. Appl. Phys.* **29,** L 566 (1990).
6. T. Siegrist, M. Zahurak, D. M. Murphy, and R. S. Roth, *Nature* **334,** 231 (1988).
7. D. Van Dyck, J. Danckaert, W. Coene, E. Selderslaghs, D. Broddin, J. Van Landuyt, S. Amelinckx, *in* "Computer Simulation of Electron Microscope Diffraction and Images" ed. by (W. Krakow and M. O'Keefe, Eds.), pp. 107–134, The Minerals, Metals, Materials series, TMS (1989).
8. D. Van Dyck and W. Coene, *Ultramicroscopy* **15,** 29 (1984).
9. H. Q. Ye and S. Amelinckx, *J. Solid State Chem.* **61,** 8 (1986).